# THE EXTREMUM SEEKING CONTROL BASED ON BAND PASS FILTER FOR THE DITHER SIGNAL PROCESSED IN THE CONTROL LOOP

**N. Bizon [1,2]    M. Oproescu [1]    M. Raducu [1]    L.M. Constantinescu [1]**

*1. Department of Electronics, Computers and Electrical Engineering, University of Pitesti, Pitesti, Romania*
*nicu.bizon@upit.ro, moproescu@yahoo.com, marian.raducu@upit.ro, luminita.constantinescu@upit.ro*
*2. University Politehnica of Bucharest, Bucharest, Romania, nicubizon@yahoo.com*

**Abstract-** In this paper an analysis of the classical high-order Extremum Seeking Control (ESC) scheme is presented in comparison with an improved ESC variant proposed here. The proposed ESC scheme is based on a band-pass filter instead of the series combination of high-pass and low-pass filters used in the classical ESC scheme. The relation between the search speed and the derivatives of the unknown input-to-output map and the cut-off frequencies of the band-pass filter is shown. The analytical results are validated by the simulation performed. Also, the ratio of the search speed is estimated analytically during the search speed based on the derivatives of the unknown input-to-output map. The performance of the proposed ESC scheme related to the search speeds is clearly highlighted in this paper based on the ratio of these search speeds that are computed and estimated by simulation, too.

**Keywords:** Nonlinear Dynamic Plant, Extremum Seeking Control, Search Speed, Renewable Energy Sources, Maximum Power Point (MPP), MPP Tracking (MPPT).

## I. INTRODUCTION

In general, a nonlinear dynamic plant has an unknown input-to-output map, $y = f(x)$, having one or more extremes (maximums or minimums). Usually, in the stationary regime, the energy sources such as renewable (Photovoltaic (PV) panels, Wind Turbines (WT), etc.) or Fuel Cells (FC) type have only one Maximum Power Point (MPP) related to the control variable used (the current or voltage) [1, 2] (Figure 1). This MPP must be tracked in dynamic regime, too [3, 4].

The MPP tracking (MPPT) algorithms were intensively developed for different areas of the PV panels [5]. The nonlinear behavior of the PV systems in shading conditions could generate rapid variations of the MPP (with solar irradiance level and temperature) that can generate multiple extremes, which complicates the tracking of the global MPP. A variety of MPPT algorithms have been proposed and implemented in the last decades. The review paper [6] introduces a classification scheme for the MPPT methods based on three categories: offline, online and hybrid methods.

In other review [7] MPPT algorithm are classified as conventional, computational methods (based on models), and soft computing techniques (based on artificial intelligence algorithms). Those classifications may be easily extended to other types of energy sources based on the reported applications for the WT [8] and FC [9].
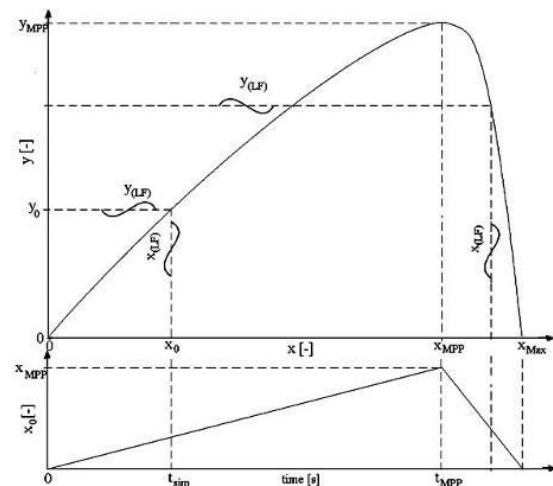


Figure 1. Searching of the MPP based on dither signal ESC scheme

Note that from the first group, which is usually referred as the conventional MPPT algorithms, the most popular three methods (together with their variations) are the Perturb and Observe (P&O) [10], the Incremental Conductance (IC) [11] and the Hill Climbing (HC) [12]. All of the above mentioned MPPT methods use fixed or variable small iteration steps to track the MPP, which finally set the values for the accuracy and search speed indicators. Note that these performance indicators typically require opposite design values for the iteration steps. Thus, if the step-size is decreased to obtain a higher tracking accuracy, then the searching speed will be lower and vice versa.

Therefore, the advanced MPPT techniques usually try to solve this by using a more complex algorithm. Anyway, even if high values are obtained for the search speed based on computational method, the tracking accuracy is still dependent on the model used [5].

The group of soft computing techniques includes Artificial Intelligence (AI) algorithms such as the Fuzzy Logic Controller (FLC) [13], Artificial Neural Network (ANN) [14] and Evolutionary Algorithms (EA) [15]. As it was mentioned before, these AI-based MPP tracking algorithms are used to optimize the MPPT operation related to the search speed [15], level of tracking oscillations [16] and robustness under variable irradiation [17]. These AI-based MPP tracking algorithms are of interest in the multi-modal problem that appears in the dynamic regime for an energy source stack obtained by series and parallel connection of the basic components.

Beside these, there are other MPPT algorithms, described in literature, based on real-time optimization methods such as the Ripple Correlation Control (RCC) [18] and ESC [19] schemes. These MPPT schemes are based on an injected signal, which is named dither, or on a ripple that normally overlaps on the power signal of energy source: (1) the low frequency (LF) ripple and (2) the high frequency (HF) ripple, having harmonics at multiples of the grid and switching frequency.

The analysis performed in this paper is focused on the performance of the ESC schemes.

It is known that the use of the classical ESC schemes can not solve the performance problem for both indicators: it is impossible to simultaneously obtain a high search speed and a good tracking accuracy [20]. Consequently, advanced ESC schemes were reported in literature [21, 22]. The main classes of ESC approaches are perturbation-based [23] and model-based methods [24].

This paper will concern itself with the ESC schemes discussed in [25, 26], being focused only on the analysis of the Band Pass Filter ESC (bpfESC) scheme, used to evaluate the search speed. In the above mentioned references a real-time optimization method based on the ESC scheme is proposed to increase both search speed and tracking accuracy indicators, related to the use of an energy source such as a PV panel [25] or a FC stack [26].

The paper is organized as follows. Section 2 presents the classical High-Order ESC (hoESC) and bpfESC schemes used in simulation. If the transfer function of the BP filter from the bpfESC scheme is equivalent with the series combination of the High-Pass (HP) and Low-Pass (LP) filters from the ho ESC scheme, then the hoESC and bpfESC schemes are functionally equivalent, too. This aspect is briefly shown in this section.

Section 3 deals with signal processing in the loop of the bpfESC scheme. An analytical analysis of the bpfESC scheme in the frequency domain is presented in this section. The main results obtained on the evaluation of the search speed are shown for both ESC schemes, too. Section 4 deals with the analytical estimation of the speeds ratio during the search phase. The comparative results are shown in Section 5 using both ESC schemes applied on three know input-to-output map. The performance of the bpfESC scheme related to the search speed is clearly highlighted in this section based on the shown simulation results. The last section concludes the paper.

## II. ON THE EQUIVALENCE OF THE HOESC AND BPFESC SCHEMES

Only using the measurements of the plant output, $y$ (for example, the power signal of the energy sources), the ESC schemes performs a tuning of the plant input, $x$, so that $y = f(x)$ is either minimized or maximized (Figure 1). The initial value, $x_0$, must be set in the region of the MPP attraction (see Figure 2) to assure $y \rightarrow y_{MPP}$, even if the noise level, $n$, is high. The analysis of the hoESC (Figure 3) and bpfESC (Figure 4) schemes is performed in this section. It can be observed that both ESC schemes have the same operating relationships, excepting the signal filtering and demodulation [20, 24, 25].
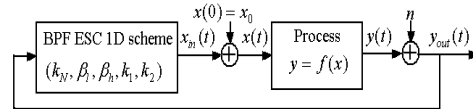


Figure 2. BPF extremum seeking control (bpfESC) scheme operating in closed loop
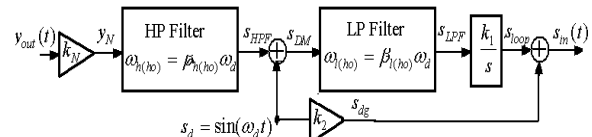


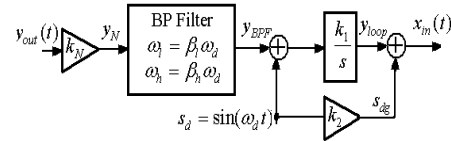Figure 3. Higher order extremum seeking control (hoESC) scheme



Figure 4. BPF extremum seeking control (bpfESC) scheme

For brevity, only relationships of the bpfESC scheme are shown below, considering $G_{BPF}(s) = G_{HPF}(s) \cdot G_{LPF}(s) = [Y_{BPF}(s)/Y_F(s)] \cdot [Y_F(s)/Y_N(s)] = [s/(s+\omega_h)] \cdot [\omega_l/(s\omega_l)]$:

$$y = f(x), \ y_{out} = y + n, \ y_N = k_N \cdot y_{out} \quad (1)$$

$$\dot{y}_F = -\omega_h y_F + \omega_h y_N, \ y_{BPF} = y_N - y_F, \quad (2)$$
$$\dot{y}_{BPF} = -\omega_l y_{BPF} + \omega_l y_F, \ y_{DM} = y_{BPF} \cdot \sin(\omega_d t)$$

$$\dot{y}_{loop} = k_1 y_{DM} \quad (3)$$

$$x \cong x_{in} + x_0, \ x_{in} = y_{loop} + s_{dg}, \ s_{dg} = k_2 \cdot \sin(\omega_d t) \quad (4)$$

where Equations (1), (3), and (4) represent the input-to-output map, the integrator, the MPP current controller based on $x_{in}$ reference, and Equations (2) represent the signal processing based on BPF and demodulation.

The following notations are used (Figure 4):
- $k_1$ is the loop gain;
- $k_2$ is the gain of the dither amplitude;
- $\omega_d$ is the frequency of the dither signal;
- $\omega_l = \beta_l \omega_d$, $0 < \beta_l < 6$, is the cut-off frequency of the LPF;
- $\omega_h = \beta_h \omega_d$, $0 < \beta_h < 1$, is the cut-off frequency of the HPF;
- $y_N$ is the signal after normalization (to the maximum value of $y$, $y_{MPP}$);
- $y_F$ is an intermediate variable related to HPF operating;
- $y_{BPF}$ is the output signal from the BPF;
- $y_{DM}$ is the signal after demodulation;
- $y_{loop}$ is the output signal from the ESC loop;
- $x_{in}$ is the estimation signal of the unknown parameter;

Relationships of the hoESC scheme related to signal processing based on BP & HP filters and demodulation are:

$$\dot{s}_F = -\omega_h s_F + \omega_h s_N \ , \ s_{HPF} = s_N - s_F \ ,$$
$$\dot{s}_{LPF} = -\omega_l s_{LPF} + \omega_l s_{HPF} \sin(\omega t) \quad (2')$$

where $s_N$, $s_{HPF}$, and $s_{LPF}$ are the signals after normalization, HPF, and LPF.

If $G_{BPF}(s) = G_{HPF(ho)}(s) \cdot G_{LPF(ho)}(s)$, then:

$$\left| G_{BPF}(\omega) \right| = \left| G_{HPF(ho)}(\omega) \right| \left| G_{LPF(ho)}(\omega) \right| ,$$
$$\phi_{BPF(ho)}(\omega) = \arg(G_{BPF(ho)}) = \phi_{HPF(ho)}(\omega) + \phi_{LPF(ho)}(\omega) \quad (5)$$

where,

$$\left| G_{HPF(ho)}(\omega) \right| = 1 / \sqrt{1 + \left( \omega_{h(ho)} / \omega \right)^2} ,$$
$$\phi_{HPF(ho)}(\omega) = \arg(G_{HPF(ho)}) = \arctan\left( (\beta_{h(ho)} \omega_d) / \omega \right) \quad (6)$$

$$\left| G_{LPF(ho)}(\omega) \right| = 1 / \sqrt{\left( \omega / \omega_{l(ho)} \right)^2 + 1} ,$$
$$\phi_{LPF(ho)}(\omega) = \arg(G_{LPF(ho)}) = -\arctan\left( \omega / (\beta_{l(ho)} \omega_d) \right) \quad (7)$$

In this case, it was shown in [25] that the absolute ratio of the search speed values ($K_{SS(bpf)}$ and $K_{SS(ho)}$, respectively) is:

$$R_{SS} = \left| K_{SS(bpf)} / K_{SS(ho)} \right| =$$
$$= \left| \cos(\phi_{HPF(ho)} + \phi_{LPF(ho)}) \right| / \cos(\phi_{HPF(ho)}) \quad (8)$$

If

$$0 < \beta_{h(ho)} < 1 < 3 < \beta_{l(ho)} \quad (9)$$

then

$$1 < R_{SS} \leq 1 / \cos(\phi_{HPF(ho)}) \leq 1.0541 \quad (10)$$

the equality being when:

$$\phi_{HPF(ho)} = \left| \phi_{LPF(ho)} \right| \Leftrightarrow \beta_{l(ho)} \cdot \beta_{h(ho)} = 1 \quad (11)$$

Thus, if $G_{BPF}(s) = G_{HPF(ho)}(s) \cdot G_{LPF(ho)}(s)$, then the hoESC (Figure 3) and the bpfESC (Figure 4) schemes have almost the same search speed. So, from this point of view, the hoESC and the bpfESC schemes are functionally equivalent. It was shown in [25] that almost the same tracking accuracy is obtained.

Relationships (11) also define the condition to have the highest value of the search speed, $K_{SS(bpf)}$. It is important to know how much the search speed is improved for the bpfESC schemes, $K_{SS(bpf)}$, in comparison with basic hoESC (bhoESC) schemes, $K_{SS(bho)}$.

If identical HP filters will be considered in both bpfESC and bhoESC schemes, which means identical cut-off frequencies:

$$0 < \beta_{h(bho)} = \beta_{h(bpf)} < 1 \quad (12)$$

then the absolute ratio of the search speed values ($K_{SS(bpf)}$ and $K_{SS(bho)}$, respectively) is:

$$R_{SS(b)} = \left| K_{SS(bpf)} / K_{SS(bho)} \right| \cong \left| G_{LPF(bpf)} \right| / \left| G_{LPF(bho)} \right| \quad (13)$$

If

$$0 < \beta_{l(bho)} < 1 < 3 < \beta_{l(bpf)} \quad (14)$$

then

$$\left( \beta_{l(bpf)} / \sqrt{\beta_{l(bpf)}^2 + 1} \right) \geq 0.95 \quad (15)$$

Thus, following average approximation can be used [24]:

$$R_{SS(b)} \cong \sqrt{1 + 1 / \beta_{l(bho)}^2} \quad (16)$$

In the next section a better approximation will be developed based on the signal processing in the bpfESC loop.

## III. SIGNAL PROCESSING IN THE BPFESC LOOP

The probing signal related to the input-output map, $y = f(x)$, can be approximated by the Taylor series:

$$y(x) = \sum_{i=0}^{\infty} \frac{(x - x_0)^i}{i!} \cdot \frac{d^i f}{dx^i}(x_0) \quad (17)$$

where $(x_0, y_0 = f(x_0))$ is a point on the static power map, which slowly varies in time as it is shown in Figure 1. If the start point is considered the point (0, 0), then the ramp for $t < t_{MPP}$ is given by relationship:

$$x_0(t) = \frac{x_{MPP}}{t_{MPP}} \cdot t = G \cdot t \quad (18)$$

Note that $t_{MPP}$ is the time of simulation and $G$ is the slope of the ramp used to test the nonlinear plant in open loop or it is the gradient that is estimated in closed loop, $K_{SS}$. In both cases, the derivatives can be computed during the simulation based on relationship:

$$\frac{df}{dx}(x_0) = \frac{df}{dt} / \frac{dx}{dt} \cong G^{-1} \cdot f^{(1)}(t) \quad (19)$$

In general:

$$\frac{d^i f}{dx^i}(x_0) \cong G^{-i} \frac{d^i f}{dt^i}(t) = G^{-i} f^{(i)}(t) \quad (20)$$

The main LF components in the bpfESC loop are set by the frequencies band of the BPF:

$$x_{LF}(t) = \sum_{j=1}^{[\beta_l]} a_j \sin(j\omega_d t) \quad (21)$$

where, considering (13), the integer $[\beta_l]$ can be set higher than 3. The magnitudes of the LF components, $a_j$, are lower than the $x_0$ value, so:

$$x = x_0 + x_{LF} \cong x_0 \quad (22)$$

and

$$\frac{dx}{dt} \cong \frac{dx_0}{dt} \quad (23)$$

Consequently:

$$y_{BPF}(t) \cong k_N \sum_{i=1}^{\infty} \left\{ \left[ \sum_{j=1}^{[\beta_l]} a_j \sin(j\omega_d t) \right]^i \frac{G^{-i} f^{(i)}(t)}{i!} \right\} \quad (24)$$

### A. Estimation of the Search Speed in the bpfESC Loop

Estimation of the search speed in the bpfESC closed loop will be performed considering the following assumptions:
- only three components of the Taylor series will be considered;
- the BPF is ideal, having $\beta_{h(bpf)} = 0.5$ and $\beta_{l(bpf)} = 3.5$;
- $G = 1$ and $k_N = 1$.
Under these conditions the relationship (24) will become:

$$y_{BPF}(t) \cong \sum_{i=1}^{3} \left\{ \left[ \sum_{j=1}^{3} a_j \sin(j\omega_d t) \right]^i \frac{f^{(i)}(t)}{i!} \right\} \qquad (25)$$

If superposition technique will be considered, then the relation (25) will be written as:

$$y_{BPF}(t) \cong \sum_{i=1}^{3} \left\{ \left[ \sum_{j=1}^{3} a_j^i \sin^i(j\omega_d t) \right] \frac{f^{(i)}(t)}{i!} \right\} \qquad (26)$$

The signal after the demodulation

$$y_{DM}(t) = y_{BPF}(t) \cdot \sin(\omega_d t) \qquad (27)$$

can be written as:

$$y_{DM}(t) \cong k_{sg} + \sum_{j=1}^{3} \left[ b_j \sin(j\omega_d t) + c_j \cos(j\omega_d t) \right] \qquad (28)$$

where,

$$k_{sg} = \frac{f^{(1)}(t) \cdot a_1}{2} + \frac{f^{(3)}(t) \cdot a_1^3}{16} \qquad (29)$$

and

$$b_1 = \frac{f^{(2)}(t) \cdot a_1^2}{8},$$

$$c_1 = \frac{f^{(1)}(t) \cdot a_2}{2} + \frac{f^{(3)}(t) \cdot a_2^3}{16},$$

$$b_2 = 0,$$

$$c_2 = \frac{f^{(1)}(t) \cdot (a_1 - a_3)}{2} + \frac{f^{(3)}(t) \cdot (4 \cdot a_1^3 - 3 \cdot a_3^3)}{48}, \qquad (30)$$

$$b_3 = \frac{f^{(2)}(t) \cdot (a_2^2 - a_1^2)}{8},$$

$$c_3 = -\frac{f^{(1)}(t) \cdot a_2}{2} - \frac{f^{(3)}(t) \cdot a_2^3}{16}$$

The $k_{sg}$ parameter will be computed in simulation based on next relationship:

$$k_{sg} = \frac{a_1}{2} \cdot \frac{df}{dx}(x_0) + \frac{a_1^3}{16} \cdot \frac{d^3 f}{dx^3}(x_0) \qquad (29')$$

Relationships (30) can be used to estimate the harmonics magnitudes in the bpfESC open loop, but to accurately compute these magnitudes in the closed loop these relationships must be rewritten considering the derivates as above.

The signal injected in the loop will be:

$$y_{loop}(t) = k_1 \int y_{DM}(t)dt \cong k_1 k_{sg} \cdot t +$$

$$+ \sum_{j=1}^{3} \left[ \frac{k_1 c_j}{j\omega_d} \sin(j\omega_d t) - \frac{k_1 b_j}{j\omega_d} \cos(j\omega_d t) \right] \qquad (31)$$

The loop gain, $k_1$, is set proportional to the dither frequency in order to assure the dither persistence in the ESC loop. So, if

$$k_1 = \gamma_{sd} \cdot \omega_d \qquad (32)$$

then

$$y_{loop}(t) \cong K_{SS(bpf)} \cdot t + \sum_{j=1}^{3} \left[ H_j \sin(j\omega_d t + \varphi_j) \right] \qquad (33)$$

where $K_{SS(bpf)}$ and $H_j$ are the estimated values for the search speed in the closed loop and the magnitude of the $j$-harmonic, respectively:

$$K_{SS(bpf)} = k_{sg} \cdot \gamma_{sd} \cdot \omega_d$$

$$H_j = \frac{\gamma_{sd}}{j} \cdot \sqrt{b_j^2 + c_j^2} \qquad (34)$$

Note that $K_{SS(bpf)}$ and $H_j$ parameters are time variables based on relationships (29) and (30).

**B. Estimation of the Search Speed in the bhoESC Loop**

The estimation of the search speed in the bhoESC closed loop will be performed considering the same assumptions as above, excepting that $\beta_{h(bho)} = 1.5$.

The LF components in the bhoESC loop are LP filtered, thus only the first harmonic will be considered:

$$x_{LF}(t) = a_1 \sin(\omega_d t) \qquad (35)$$

The signal after the HPF is:

$$s_{HPF}(t) \cong a_1 \frac{df}{dx}(x_0) \cdot \sin(\omega_d t) \qquad (36)$$

Thus, the signal after demodulation can be written as:

$$s_{DM}(t) = s_{HPF}(t) \cdot \sin(\omega_d t) \cong$$

$$\cong a_1 f^{(1)} \cdot \sin^2(\omega_d t) = \qquad (37)$$

$$= a_1 f^{(1)} / 2 - a_1 f^{(1)} \cdot \cos(2\omega_d t) / 2$$

Under the assumption mentioned above, the signal after the LPF will be:

$$s_{LPF}(t) \cong a_1 f^{(1)} / 2 \qquad (38)$$

$$s_{loop}(t) = k_1 \int s_{LPF}(t)dt \cong \left( k_1 a_1 f^{(1)} / 2 \right) \cdot t = K_{SS(bho)} \cdot t \qquad (39)$$

where,

$$K_{SS(bho)} = k_1 a_1 f^{(1)} / 2 = \gamma_{sd} \omega_d \frac{a_1}{2} \cdot \frac{df}{dx}(x_0) \qquad (40)$$

**IV. ESTIMATION OF THE SPEEDS RATIO DURING THE SEARCH PHASE**

The ratio of the search speed values can be estimated based on relationship (35) and (40) as below:

$$R_{SS(b)}(t) = \frac{K_{SS(bpf)}}{K_{SS(bho)}} \qquad (41)$$

Because the magnitude of the first harmonic, $H_1$, for the $y_{BPF}$ signals varies during the simulation in the closed loop, this magnitude will be estimated using the Fast Fourier Transform (FFT).

Thus, in the closed loop, relationship (41) became:

$$R_{SS(b)}(t) = 1 + \left| \frac{df^3}{dx^3}(x_0) / \frac{df}{dx}(x_0) \right| \cdot \frac{H_1^2(t)}{8} \qquad (42)$$

The computing block of the MATLAB-SIMULINK® diagram (see Figure 5) estimates the absolute ratio of the search speed values based on (42). This diagram is used for comparative tests of the hoESC and bpfESC schemes in closed loop, considering different know input-output maps, $y_p = f_p(x) = 1 - (1 - x)^{2p}$, $p=1, 2, 3$. Some simulation results will be shown in next section.
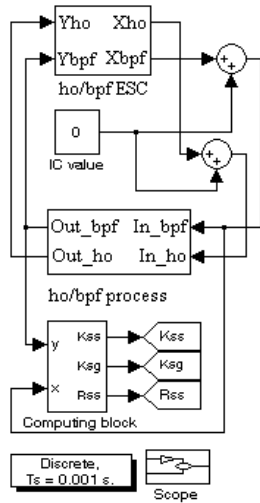
Figure 5. The diagram for comparative tests of the hoESC and bpfESC schemes using the same process in the closed loop

## V. SIMULATION RESULTS

The following parameters are used for bpfESC schemes in all simulations: $\gamma_{sd} = 0.2$ ($k_1 = 2\pi\gamma_{sd}f_d$), $\beta_{h(bpf)} = 0.18$ and $\beta_{l(bpf)} = 5.5$. Besides these, two values are used for the dither frequency ($f_d$) and for the gain of the dither magnitude ($k_2$) to highlight some analytical results using the simulation performed. The used values for the dither are mentioned in each case.

The derivatives for the input-output maps considered, $y_p = f_p(x) = 1 - (1 - x)^{2p}$, $p = 1, 2, 3$, are:

$$y_p^{(1)}(x_0) = \frac{df}{dx}(x_0) = 2p(1 - x_0)^{2p-1}, \quad p = 1, 2, 3$$

$$y_p^{(3)}(x_0) = \frac{d^3 f}{dx^3}(x_0) = \tag{43}$$

$$= 2p(2p-1)(2p-2)(1 - x_0)^{2p-3}, \quad p = 2, 3$$

$$y_1^{(3)}(x_0) = 0, \quad p = 1$$

These relationships were used in the computing block for both ESC schemes. Firstly, some simulations are presented in Figure 6 related to the search phase for the bhoESC (●) and bpfESC (■) schemes with $k_2 = 0.001$, using $f_d = 50$ Hz (case a), and $f_d = 5$ Hz (case b). As it was expected based on (1), the convergence time is proportional with dither frequency.

Looking to the zooms shown in Figure 7 at $t = 0.2$ s (case a), and $t = 2$ s (case b), the ratio of the search speeds can be estimated for each of the input-output maps, $y_p = f_p(x)$, as being about 1, 1.3, and 1.8 for $p = 1$, 2, and 3, respectively. Note that the average value computed based on (16) is 1.2 and 2.2, for the $\beta_{l(bho)}$ value of 1.5 and 0.5, respectively.

The search speed computed based on (34) and (29') is shown in Figure 8 for the same cases and parameters mentioned above. The simulation results shown in Figure 8 validate the analytical results presented above for the bpfESC scheme:
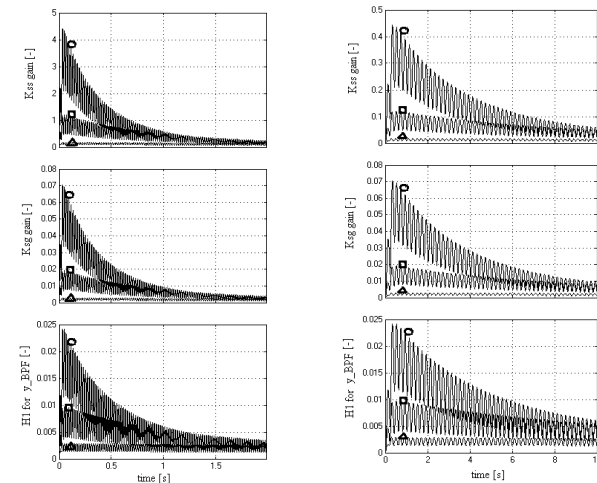
- The shape of the $K_{SS(bpf)}$ (top), $k_{sg(bpf)}$ (middle) and $H_1$ (bottom) parameters during the search phase is the same (Figure 8).
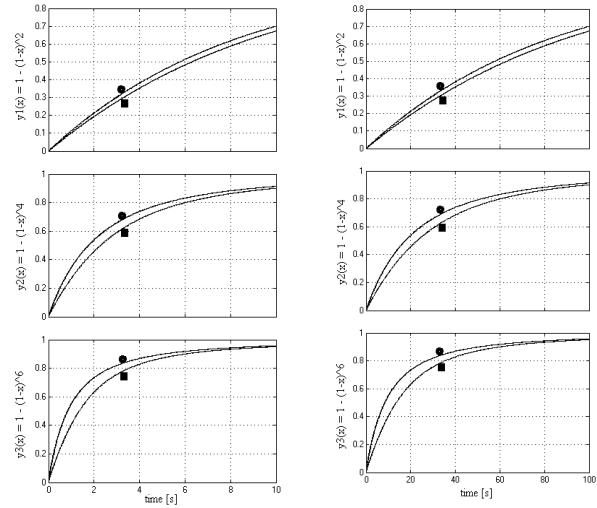


a) $f_d = 50$ Hz          b) $f_d = 5$ Hz

Figure 6. The search phase for the bhoESC (●) and bpfESC (■) schemes with $\gamma_{sd} = 0.2$ ($k_1 = 2\pi f_d$), $k_2 = 0.001$, $\beta_{l(bho)} = 1.5$, $\beta_{h(bpf)} = 0.18$ and $\beta_{l(bpf)} = 5.5$
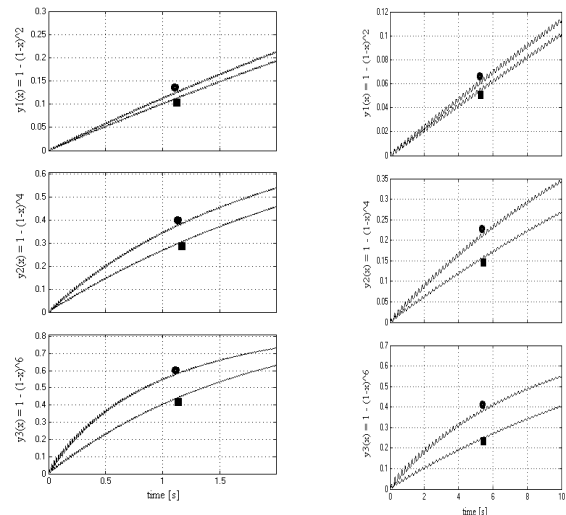


a) $f_d = 50$ Hz          b) $f_d = 5$ Hz

Figure 7. Zooms of the search phase for the bhoESC (●) and bpfESC (■) schemes with $\gamma_{sd} = 0.2$ ($k_1 = 2\pi\gamma_{sd}f_d$), $k_2 = 0.001$, $\beta_{l(bho)} = 1.5$, $\beta_{h(bpf)} = 0.18$ and $\beta_{l(bpf)} = 5.5$



a) $f_d = 50$ Hz          b) $f_d = 5$ Hz

Figure 8. $K_{SS(bpf)}$ (top), $k_{sg(bpf)}$ (middle) and $H_1$ (bottom) during the searching phase for the bpfESC scheme with $\gamma_{sd} = 0.2$ ($k_1 = 2\pi\gamma_{sd}f_d$), $k_2 = 0.001$, $\beta_{h(bpf)} = 0.18$ and $\beta_{l(bpf)} = 5.5$, and different input-output map, $y_p = 1 - (1 - x)^{2p}$, $p=1$ (●), 2 (■), 3 (△) and

- The average value of the $k_{sg(bpf)}$ (middle) and $H_1$ (bottom) parameters is almost the same for both frequencies.

- The initial value for the $k_{sg(bpf)}$ parameter is about 0.07 (for $p = 3$) and 0.018 (for $p = 2$) in both cases. Also, the initial value for the $H_1$ magnitude is about 0.024 (for $p = 3$) and 0.09 (for $p = 2$) in both cases. On the other hand, considering the above comments and the value of $a_1 = H_1$, the initial value for the $k_{sg(bpf)}$ parameter can be estimated based on (29') as:

$$k_{sg}(0) \cong \frac{a_1}{2} \cdot \frac{df}{dx}(0) = p \cdot H_1 \qquad (44)$$

It is easy to notice that the above simulation results validate the relationship (44).

- Other values for the simulated $k_{sg(bpf)}$ parameter can be estimated based on (29') and (44), too. Thus, the analytical result given by (34), related to the $k_{sg(bpf)}$ parameter, is validated through simulation.

- Also, considering $\gamma_{sd} = 0.2$ and $f_d = 50$ Hz (case a), the initial value for the $K_{SS(bpf)}$ indicator is about 0.7 (for $p = 3$) and 0.18 (for $p = 2$). Thus, considering the initial value for the simulated $k_{sg(bpf)}$ parameter mentioned above, the $\gamma_{sd}$ parameter can be estimated based on (40) as $4.4/(314 \cdot 0.07) \cong 0.2$ (for $p = 3$) and $1.2/(314 \cdot 0.018) \cong 0.21$ (for $p = 2$).

- It is easy to notice that the values for the $K_{SS(bpf)}$ indicator are 10-times lower in case b, when the dither frequency is set to be 10-times lower than in case a. Thus, the analytical result given by (40), related to the $K_{SS(bpf)}$ indicator, is validated through simulation.

Secondly, some simulations related to the search phase for the bpfESC schemes using a $k_2$ gain ($k_2=0.1$), which is 100-times higher than the above value, are presented in Figure 9, to highlight the second term of the relationship (29'). The $k_1$ loop gain is set 10-times lower ($\gamma_{sd} = 0.02$, $f_d = 50$ Hz) than the above value to assure the loop stability.
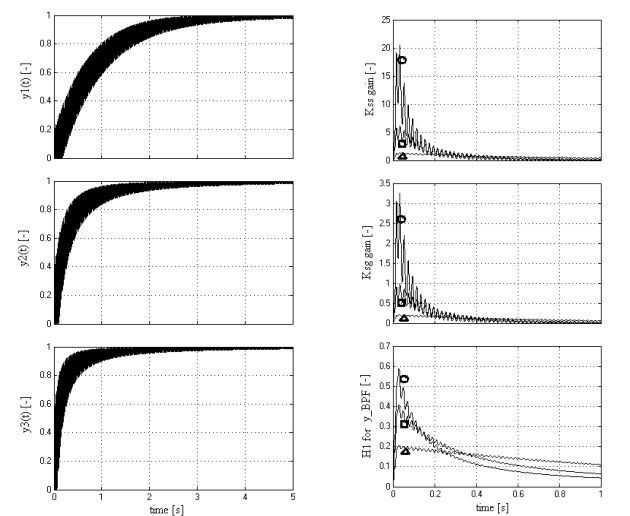


a) The search phase for different input-output map, $y_p = 1 - (1 - x)^{2p}$, $p = 1$ (top), 2 (middle), 3 (bottom)

b) $k_{sg(bpf)}$ (top), $K_{SS(bpf)}$ (middle) and $H_1$ (bottom) for different input-output map, $y_p = 1 - (1 - x)^{2p}$, $p = 1$ (⬤), 2 (◻), 3 (△)

Figure 9. The bpfESC scheme with $\gamma_{sd} = 0.02$ ($k_1 = 2\pi f_d$), $k_2 = 0.1$, $f_d = 50$ Hz, $\beta_{h(bpf)} = 0.18$ and $\beta_{l(bpf)} = 5.5$

The simulation results validate the analytical results presented above for the bpfESC scheme:

- As it was expected based on (40), the convergence time is proportional with the product of the frequency and magnitude of dither. The convergence time is 10-times lower in Figure 10 than in Figure 7(a).

- Considering the initial value for the $K_{SS(bpf)}$ indicator and $k_{sg(bpf)}$ parameter, the $\gamma_{sd}$ parameter can be estimated based on (34) as $20/(314 \cdot 3) \cong 0.021$ (for $p = 3$) and $6/(314 \cdot 0.9) \cong 0.021$ (for $p = 2$). Thus, the analytical result given by (34) is further validated through simulation.

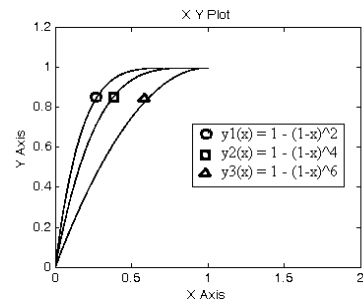The search phase is shown in the Y-X phase plane (Figure 10) for different $y_p = 1 - (1 - x)^{2p}$.



Figure 10. The search phase is shown in the Y-X phase plane for different $y_p = 1 - (1 - x)^{2p}$, $p = 1$(⬤), 2(◻), 3(△)

The ratio of the search speed values can be estimated based on relationship (42), but also by the simulation shown in Figure 11.
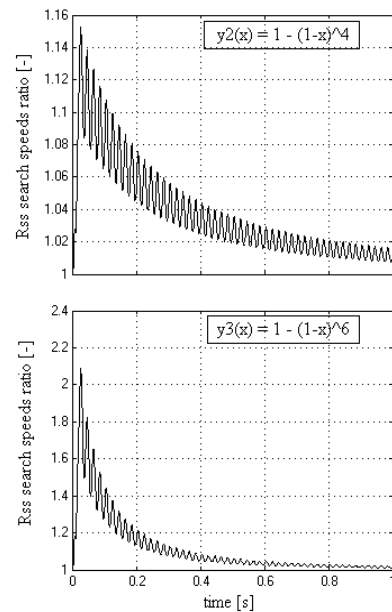


Figure 11. The ratio of the search speed values for the bpfESC scheme with $\gamma_{sd} = 0.02$ ($k_1 = 2\pi f_d$), $k_2 = 0.1$, $f_d = 50$ Hz, $\beta_{h(bpf)} = 0.18$ and $\beta_{l(bpf)} = 5.5$, and different $y_p = f(x) = 1 - (1 - x)^{2p}$, $p = 2$(top), 3(bottom)

The simulation results validate the analytical results obtained based on (43):

- Case $p = 3$: the initial ratio of the search speed is $1+(120/6) \cdot (0.6)^3/8=1.9$; the initial ratio computed from the simulation results is about 2.

- Case $p = 2$: the initial ratio of the search speed is $1+(24/4) \cdot (0.4)^3/8=1.12$; the initial ratio computed from the simulation results is about 1.14.
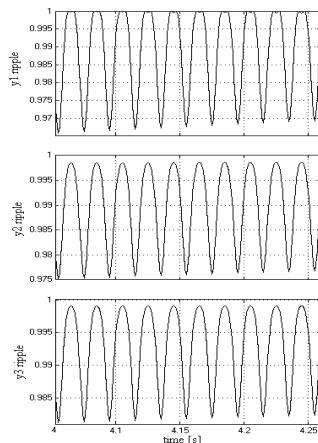
Figure 12. Ripple during the stationary phase for the bpfESC scheme with $\gamma_{sd} = 0.02$ ($k_1 = 2\pi\gamma_{sd}f_d$), $k_2 = 0.1$, $f_d = 50$ Hz, $\beta_{l(bpf)} = 0.18$, $\beta_{h(bpf)} = 5.5$, and different $y_p = 1 - (1 - x)^{2p}$, $p = 1$(top), 2(middle), 3(bottom)

Note that the dither has a higher magnitude during the search phase (bottom plot in Figure 8(b)). The ripple during the stationary phase is shown in Figure 12.

The ripple measured during the stationary phase (around $t = 4$ s) is about 3.5% (for $p = 1$), 2.5% (for $p = 2$), 2% (for $p = 3$). So, even if the period of the stationary phase is long enough, the ripple is higher than 2%. For example, if a PV panel has 10 kW power, then the power ripple is higher than 200 W, which means a lot from point of view of energy efficiency. As it was mentioned, a solution to improve the tracking accuracy was proposed in [25].

## VI. CONCLUSIONS

Besides the well known results that are also available for the proposed ESC scheme, such as the result about the convergence time (which is proportional with the product of the frequency and the magnitude of the dither), some new results related to the ESC scheme are shown in the first sections of this paper. The promising outcomes from this work are listed below. Note that these must be interpreted in the context of the modelling approach used. The analytical analysis was kept at a simple level in order to gain an initial understanding of the signal processing in the ESC loop. The main analytical results are: (1) the search speed values were estimated for both ESC schemes based on the derivatives of the unknown input-output map; (2) the relationships to compute the harmonics magnitudes during the search phase were given; (3) the ratio of the search speed values can be computed during the search phase.

All the analytical results shown were validated here by simulation. The main results are: (1) the search speeds that were estimated analytically based on the derivatives are also computed in simulation to validate the theoretical results; (2) the mean value of the speeds ratio during search speed was computed, validating that this is close to the average approximation of this ratio based on a frequency approach [26]; (3) the dither persistence is dependent to the cut-off frequencies of the band-pass filter; (4) the performance benefits arise from the greater flexibility of the bpfESC scheme.

## REFERENCES

[1] M. Dargahi, J. Rouhi, M. Rezanejad, M. Shakeri, "Maximum Power Point Tracking for Fuel Cell in Fuel Cell/Battery Hybrid Power Systems", European J. Sci. Res., Vol. 25, No. 4, pp. 538-548, 2009.

[2] T. Esram, P.L. Chapman, "Comparison of Photovoltaic Array Maximum Power Point Tracking Techniques", IEEE Trans. on Energy Conver., Vol. 22, No. 2, pp. 439-449, 2007.

[3] V. Salas, E. Olias, O. Barrado, A. Lazaro, "Review of the Maximum Power Point Tracking Algorithms for Stand-Alone Photovoltaic Systems", Sol. Energ Mat. Sol., C, Vol. 90, No. 11, pp. 1555-1578, 2006.

[4] S. Caux, W. Hankache, M. Fadel, D. Hissel, "On-line Fuzzy Energy Management for Hybrid Fuel Cell Systems", Int. J. Hydrogen Energy, Vol. 35, No. 5, pp. 2134-2143, 2010.

[5] J.C. Wang, Y.L. Su, J.C. Shieh, J.A. Jiang, "High Accuracy Maximum Power Point Estimation for Photovoltaic Arrays", Sol. Energy Mat. Sol., C, Vol. 95, pp. 843-851, 2011.

[6] A.R. Reisi, M.H. Moradi, S. Jamasb, "Classification and Comparison of Maximum Power Point Tracking Techniques for Photovoltaic System: A Review", Renew. Sust. Energy Rev., Vol. 19, pp. 433-443, 2013.

[7] K. Ishaque, Z. Salam, "A Review of Maximum Power Point Tracking Techniques of PV System for Uniform Insolation and Partial Shading Condition", Renew. Sust. Energy Rev., Vol. 19, pp. 475-488, 2013.

[8] M. Dali, J. Belhadj, X. Roboam, "Hybrid Solar-Wind System with Battery Storage Operating in Grid-Connected and Standalone Mode: Control and Energy Management - Experimental Investigation", Energy, Vol. 35, No. 6, pp. 2587-2595, 2010.

[9] L.N. Khanh, J.J. Seo, Y.S. Kim, D.J. Won, "Power Management Strategies for a Grid Connected PV-FC Hybrid System", IEEE Trans. on Energy Conv., Vol. 25, No. 3, pp. 1874-1882, 2010.

[10] A. Giustiniani, et al., "Enhancing Polymeric Electrolyte Membrane Fuel Cell Control by Means of the Perturb and Observe Technique", Fuel Cell Sci. Technol., Vol. 7, No. 1, pp. 11021-11031, 2010.

[11] F. Liu, S. Duan, F. Liu, B. Liu, Y. Kang, "A Variable Step Size INC MPPT Method for PV Systems", IEEE Trans. on Ind. Electron., Vol. 55, No. 7, pp. 2622-2628, 2008.

[12] W. Xiao, A. Elnosh, V. Khadkikar, H. Zeineldin, "Overview of Maximum Power Point Tracking Technologies for Photovoltaic Power Systems", The 37th Annual Conference of IEEE IES (IECON 2011), pp. 3900-3905, 2011.

[13] F. Bouchafaa, I. Hamzaoui, A. Hadjammar, "Fuzzy Logic Control for the Tracking of Maximum Power Point of a PV System", Energy Procedia, Vol. 6, pp. 633-642, 2011.

[14] A.D. Karlis, T.L. Kottas, Y.S. Boutalis, "A Novel Maximum Power Point Tracking Method for PV Systems Using Fuzzy Cognitive Networks (FCN)", Electr. Pow. Syst. Res., Vol. 77, No. 3-4, pp. 315-327, 2007.

[15] C.C. Liao, "Genetic K-Means Algorithm Based RBF Network for Photovoltaic MPP Prediction", Energy, Vol. 35, No. 2, pp. 529-536, 2010.

[16] L.R. Chen, C.H. Tsai, Y.L. Lin, Y.S. Lai, "A Biological Swarm Chasing Algorithm for Tracking the PV Maximum Power Point", IEEE Trans. on Energy Conver., Vol. 25, No. 2, pp. 484-493, 2010.

[17] R. Kadri, H. Andrei, J.P. Gaubert, T. Ivanovici, G. Champenois, P. Andrei, "Modeling of the Photovoltaic Cell Circuit Parameters for Optimum Connection Model and Real-Time Emulator with Partial Shadow Conditions", Energy, Vol. 42, No. 1, pp. 57-67, 2012.

[18] M. Becherif, D. Hissel, "MPPT of a PEMFC Based on Air Supply Control of the Motocompressor Group", Int. J. Hydrogen Energy, Vol. 35, No. 22, pp. 12521-12530, 2010.

[19] T. Esram, J.W. Kimball, P.T. Krein, P.L. Chapman, P. Midya, "Dynamic Maximum Power Point Tracking of Photovoltaic Arrays Using Ripple Correlation Control", IEEE Trans. on Power Electron, Vol. 21, No. 5, pp. 1282-1291, 2006.

[20] K.B. Ariyur, M. Krstic, "Real-Time Optimization by Extremum Seeking Control", John Wiley and Sons, NY, 2003.

[21] G. Gelbert, J.P. Moeck, C.O. Paschereit, R. King, "Advanced Algorithms for Gradient Estimation in One- and Two-Parameter Extremum Seeking Controllers", J. Process Control, Vol. 22, pp. 700-709, 2012.

[22] F.E. Azar, M. Perrier, B. Srinivasan, "A Global Optimization Method Based on Multi-Unit Extremum Seeking for Scalar Nonlinear Systems", Comput. Chem. Eng., Vol. 35, pp. 456-463, 2011.

[23] C. Manzie, M. Krstic, "Extremum Seeking with Stochastic Perturbations", IEEE Trans. on Automatic Control, Vol. 54, pp. 580-585, 2009.

[24] M. Guay, D. Dochain, M. Perrier, "Adaptive Extremum Seeking Control of Continuous Stirred Tank Bioreactors with Unknown Growth Kinetics", Automatica, Vol. 40, pp. 881-888, 2004.

[25] N. Bizon, "Energy Harvesting from the PV Hybrid Power Source", Energy, Vol. 54, No. 1, pp. 297-307, 2013.

[26] N. Bizon, "Energy Harvesting from the FC Stack that Operates Using the MPP Tracking Based on Modified Extremum Seeking Control", Appl. Energy, Vol. 104, pp. 326-336, 2013.

## BIOGRAPHIES

**Nicu Bizon** was born in Albesti de Muscel, Arges County, Romania, 1961. He received a five-year degree in Electronic Engineering from the University "Polytechnic" of Bucharest, Romania, in 1986, and the Ph.D. degree in Automatic Systems and Control from the same university, in 1996. Firstly, he was in hardware design with the Dacia Renault SA, Romania. Currently, he is Professor with the University of Pitesti, Romania, being Dean of the Faculty of Electronics, Communication and Computers from 2012. Previously, he was the general manager of the "Muntenia" Training Centre (CFM) during 2000-2004. Also, he was head of University Research Department (2004-2008) and Executive Director of the Research Centre "Modeling and Simulation Processes and Systems" (2008-2012), being manager of two project in field of Green and Hydrogen Energy, and team member in other four projects in the same field. He is editor of six books in field of Green Energy and Advances in Energy Research. His current research interests include the broad area of nonlinear systems, on both dynamics and control applied in the green energy field. He was authored or co-authored of several papers (over to 100) in journals (ISI web of knowledge or data base indexed) or international conferences proceedings. He has expertise in field of renewable energy, being evaluator of Research Projects for FP7 Programme, EVAL-INCO Programme, EACI Programme, NSRF 2007-2013 (Greece), CNCSIS Ideas and ANCS PN II Programme (Romania).

**Mihai Oproescu** was born in Pitesti, Romania, on September 02, 1974. He completed the studies in the University of Pitesti (1998-2011) attaining a B.Sc. and a Ph.D. degree in Electrical Engineering Science with thesis "Modeling and Optimizing of Power Flows on Inverter Systems Powered by Fuel Cells". Over the last 8 years he published over 40 papers focused on renewable energy and power electronics. Currently, he is lecturer of Power Electronics at the University of Pitesti. He participated in 9 national scientific research projects: in 1 as a manager, in 2 as economic responsible, and as member in the rest. Also, he published a book in the field of green energy and 2 chapters in books published by Nova Science, USA.

**Marian Raducu** was born in Babana, Arges County, Romania, 1963. He received a five-year degree in Electronics Engineering from the University "Polytechnic" of Bucharest, Romania, in 1987, and the Ph.D. degree in Electronics and Telecommunication Engineering from the University of Pitesti, Romania in 2003. He is currently a lecturer at the University of Pitesti, being Vice-Dean of the Faculty of Electronics, Communication and Computers from 2012. He is the author of one book in Analogical Electronics area and co-author of the book chapter PWM Cycloconverter - An Energy Efficient Topology For Fuel Cell Inverter Systems of the book Advances in Energy Reserch. Energy and Power Engineering. His current research interests include the broad area of the nonlinear systems, on both dynamics and control, and power electronics. He is the author or co-author of several papers (over to 25) that have been published in journals (ISI/BDI or Romanian Academy indexed) and international conferences proceedings. He participated in

12 national scientific research projects as a team member. He is member of the organizing committee of the "Electronics, Computers and Artificial Intelligence - ECAI" Conference in 2007, 2009, 2011 editions.

**Luminita Mirela Constantinescu** was born in Slatina, Romania, in 1970. She received the B.Sc. and M.Sc. degrees from Faculty of Electrical Engineering, Technical University of Timisoara, Romania in 1994 and Ph.D. degree from Faculty of Electrical Engineering, University Politehnica of Bucharest, Romania, in 2004. She has been with the Faculty of Electronics, Communications and Computers of University of Pitesti, Romania, since 1995, where she worked first as an Assistant Professor and then, from 2001 as a lecturer. She is currently Vice-Dean of the Faculty of Electronics, Communication and Computers, from 2012. Her current research preoccupations include study of electric and magnetic circuits, of the electrical equipment of automobiles and of the hybrid power sources. She is the author or coauthor of over 45 papers published in national and international journals or conference proceedings. She is member of IEEE and AGIR - Romania.